Chaos, Solitons and Fractals 196 (2025) 116404

Contents lists available at ScienceDirect

Chaos, Solitons and Fractals

journal homepage: www.elsevier.com/locate/chaos

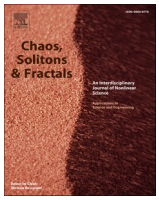

Dismantling directed networks: A multi-temporal information field approach

Min Wu, Jianhong Mou, Bitao Dai, Suoyi Tan, Xin Lu *

College of Systems Engineering, National University of Defense Technology, Changsha 410073, China

ARTICLE INFO

Keywords:
Complex networks
Network dismantling
Directed network
Information flow
Directed network entanglement

ABSTRACT

While network robustness is often assessed via structural connectivity, this approach does not fully capture the performance of complex systems, which also depends on information flow among internal components. In this paper, we focus on the robustness of directed networks by proposing a framework to dismantle both their information flow and connectivity. Specifically, we develop a multi-temporal information field model for directed networks based on quantum mechanics, and construct the Directed Node Entanglement (*DNE*) centrality metric using a generalized network density matrix. We first investigate the impact of time scale on *DNE* and find that its dismantling performance is optimal at a smaller τ. Consequently, we approximate *DNE* at these scales using mean-field theory and validate the accuracy of our approximation. Moreover, extensive targeted attack experiments on real-world networks show that *DNE* effectively disrupts both information flow and connectivity, achieving improvement rates of up to 21.34 % and 40.39 %, respectively. Finally, correlation analyses indicate that *DNE* accounts for both high outward connectivity and bridging potential, offering a distinct perspective on node importance in directed networks. In summary, our study extends the information field model to directed networks and investigates both their information flow and connectivity, providing valuable insights into network robustness.

1. Introduction

Complex systems are ubiquitous in nature and human society, emerging in domains ranging from biological networks to technological infrastructures [1–5]. Their functionality and resilience stem from intricate interactions among internal components, making it essential to understand and optimize these interactions for efficient operation [6]. Network dismantling focuses on developing methods to effectively disrupt network functionality under resource constraints [7], and it plays an important role in preventing virus propagation [8] and disrupting terrorist communications [9], among other applications.

Since a network's structure directly influences its functionality, researchers have primarily concentrated on network connectivity, especially examining how disturbances impact the size of the largest connected component (LCC) [10]. Based on LCC, numerous network dismantling algorithms have been proposed, including heuristic-based methods [7,11–13], centrality-based approaches [10,14,15], and deep reinforcement learning-based algorithms [16,17]. These approaches have made significant strides in dismantling network connectivity. However, networks can exhibit high robustness despite low connectivity, as observed in scenarios such as gene mutations in gene-gene interaction networks [18], species extinctions in ecosystems [19], router failures in the internet [20], or the unavailability of communication networks [21].

To address the limitations of focusing solely on connectivity, additional functional metrics, such as the dynamics of information flow, provide deeper insights into how local disruptions propagate throughout a network [22]. Information flow captures both the interactions among nodes and the overall dynamical properties of the system [23–25]. Furthermore, the diversity of its pathways has been shown to correlate with the sparsity observed in real-world networks [26], making it a crucial metric for evaluating network functionality. Unlike structural analysis, which focuses solely on topological connectivity, the exchange of information in complex networks depends on both the network's topology and the dynamic interactions between nodes [27], making it essential to integrate structural topology and dynamic processes into a unified analytical framework for a comprehensive understanding of network behavior [28–30]. Recent studies have combined multi-temporal diffusion processes with network topology to propose the node entanglement centrality (*CNE*) algorithm [31]. Applied to

* Corresponding author.

https://doi.org/10.1016/j.chaos.2025.116404
Received 6 March 2025; Accepted 31 March 2025

dismantle both the connectivity and information flow [32], *CNE* effectively identifies key nodes in multi-scale information propagation, showing notable advantages in reducing network functionality. Nonetheless, these studies predominantly address undirected networks, overlooking the unique challenges posed by directed networks. Since many real-world systems are inherently directed [33] —for instance, neural signal transmission in neural networks, fund transfers in financial systems, and substance exchanges in biological processes—there is a critical need for theoretical frameworks that account for edge directionality. The explicit directionality of edges in directed networks makes the dynamic processes between nodes inherently more complex, exhibiting significant heterogeneity and direction dependence. In directed networks, the dynamic processes between nodes exhibit significant heterogeneity and directional dependence, demanding novel methodologies to characterize functional robustness and unravel dynamic behaviors across different temporal scales.

In this study, we focus on the robustness of directed networks by introducing a novel approach for evaluating and dismantling both their information flow and connectivity. Specifically, we model the dynamic processes between nodes as a random walk, construct the directed network's density matrix along with the corresponding von Neumann entropy, and subsequently propose the Directed Node Entanglement (*DNE*) centrality metric. To quantify the network's information flow capacity, we introduce the Normalized Received Information (*NRI*) metric. Additionally, we compare *DNE* with benchmarks to validate its effectiveness in dismantling various real-world networks. The results reveal

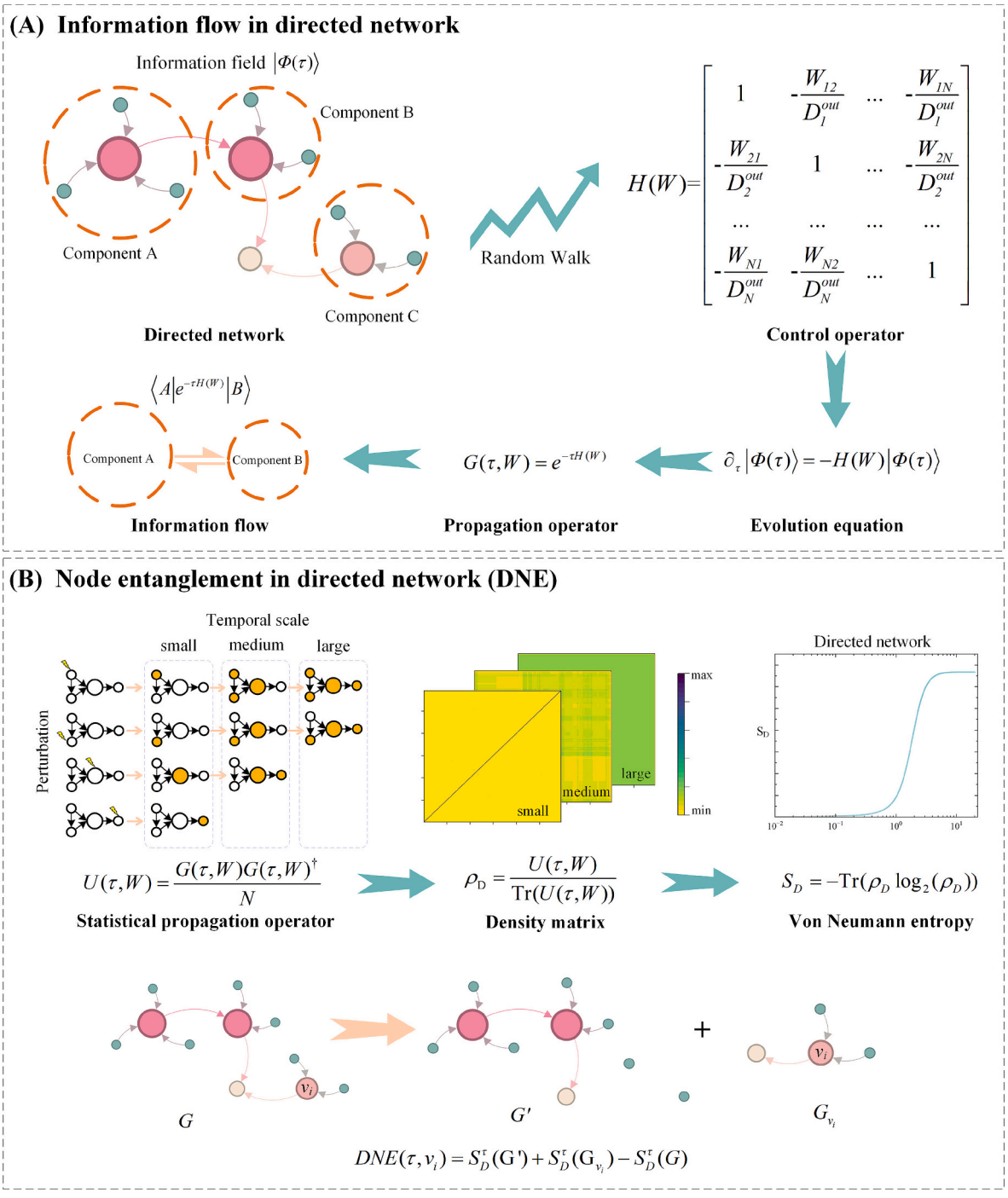

Fig. 1. (A) The information field theory for directed networks. (B) Definition of the *DNE* centrality metric.

that *DNE* can more efficiently dismantling information flow and connectivity, thereby underscoring its advantages in destroying the robustness of directed networks.

2. Data and method

2.1. Information field

Real-world systems are typically modeled as complex networks, where the elements of the system are represented as nodes and their interactions as edges. As illustrated in the Fig. 1(A), suppose the directed network possesses an information field $|\Phi(\tau)\rangle$ [22] that unifies a range of dynamical processes governing the evolution of information on top of static or time-varying structures, with τ serving as a temporal parameter that encodes the scale of information propagation. Let the information state of node v_i at τ be represented by standard canonical vectors $|v_i(\tau)\rangle$, $i = 1,2,...,N$, and the edges be encoded by a time-varying operator $W(\tau)$. Specifically, $W(\tau)$ represents the weighted and directed adjacency matrix W in the node space defined by the canonical vectors $|v_i(\tau)\rangle$ at different temporal scales, thereby capturing the dynamic properties of the network. The link from the v_i to v_j is expressed as $\langle v_i|W(\tau)|v_j\rangle$.

The information field evolves dynamically, with the flow of the field from one node to another corresponding to the exchange of information between them. The evolution of the information field is governed by a linear equation or the linearization of a nonlinear dynamical equation:

$$\frac{\partial|\Phi(\tau)\rangle}{\partial\tau} = -H(W)\Phi(\tau), \tag{1}$$

where $H(W)$ is the control operator which also serves as the Hamiltonian of the system. Given the directional nature of information flow in directed networks, our study models the network's dynamics as a random walk [34] to directly account for the propagation constraints of directed edges. The control operator is defined as:

$$H(W) = I - P, \tag{2}$$

where I is the identity matrix and P is the transition matrix of the directed network, with $P_{ij} = W_{ij}P/d_i^{out}$ representing the probability of transitioning from node v_i to node v_j. The propagation operator can be obtained as the solution to Eq. (1), expressed as $G(\tau, W(\tau)) = e^{-\tau(I-P)}$. Consequently, the information flow from node v_i to node v_j can be expressed as $\langle v_j|e^{-\tau(I-P)}|v_i\rangle$, which represents the interaction between the vector of node v_i and that of node v_j under the evolution operator $G(\tau, W)$. As τ increases, $G(\tau, W)$ encodes communication over different distances within network.

$G(\tau, W)$ not only describes the evolution of the $|\Phi(\tau)\rangle$ from its initial state to any temporal scale τ, but also encapsulates the information flow capabilities of individual nodes in the network. Specifically, $\langle v_j|e^{-\tau(I-P)}|v_i\rangle$ represents the amplitude for information to be transmitted from node v_i to node v_j at temporal scale τ, reflecting the network's information transmission capacity. The average received information (*ARI*) is a metric used to assess the information propagation ability within the network [32]. However, *ARI* does not always decrease monotonically as nodes are removed, which limits its ability to fully capture the effects of node removal. To address this issue, we use a modified metric called Received Information (*RI*), which more accurately evaluates the network's information flow capacity. Mathematically, *RI* is defined as:

$$RI = \sum_{i,j=1}^{N} \langle x_j|e^{-\tau(I-P)}|x_i\rangle(1-\delta_{ij}), \tag{3}$$

where δ_{ij} represents the Kronecker delta function ($\delta_{ij} = 1$ if $i = j$, and $\delta_{ij} = 0$ otherwise), ensuring that self-information interchange is excluded, as we focus on information transfer between nodes. The Normalized form of Received Information (*NRI*), can be expressed as:

$$NRI = \frac{RI}{RI_0}, \tag{4}$$

where RI_0 represents the information interchange capacity of the original, intact network. It worth notice that *NRI* decreases as nodes are removed. And the smaller the *NRI*, the lower the network's functional robustness.

2.2. Node entanglement in directed networks

In quantum mechanics, probability distributions are represented by density matrices. The density matrix is a Hermitian and positive semi-definite matrix with a trace equal to 1, and it is used to represent both mixed and pure states. Inspired by this concept, the network density matrix ρ is introduced [35]. Based on the information field theory discussed in the previous section, by modeling the dynamical processes within the network as diffusion, the control operator $H(W)$ can be defined as $L = D - W$, where D is the degree diagonal matrix. Consequently, the propagation operator in this model is $G(\tau, W) = e^{-\tau L}$. By normalizing the propagation operator, the density matrix can express as $\rho = e^{-\tau L}/Z$, where $Z = Tr(e^{-\tau L})$ is the trace of the $G(\tau, W)$. Notably, ρ is also a positive semi-definite matrix with a trace equal to 1, thereby conforming to the mathematical form of a quantum density matrix. Utilizing the density matrix, the von Neumann entropy of the undirected network is defined as $S_\tau = -Tr(\rho log_2\rho)$.

In directed networks, when dynamic processes are abstracted as diffusion, a key challenge lies in modifying the Laplacian matrix to serve as a control operator effectively. To address this, we model nodes interactions as a random walk process, which inherently captures the asymmetry of directed edges. By defining transition probabilities that constrain movement to designated edge directions, this approach enables a more precise assessment of influence propagation and structural vulnerability. However, this introduces a new challenge: the governing operator $H(W)$ is no longer symmetric, and the normalized propagation operator loses the positive semi-definite property characteristic of density matrices in undirected networks. Specifically, its eigenvalues may be complex, which complicates their physical interpretation. To overcome these challenges, we build upon the generalized network density matrix principle [36] and design a statistical propagation operator for directed networks as follows:

$$U(\tau, W) = \frac{G(\tau, W)G(\tau, W)^\dagger}{N}, \tag{5}$$

where $G(\tau, W)^\dagger$ is the conjugate transpose of the propagation operator $G(\tau, W)$. By normalizing the statistical propagation operator, the density matrix for directed networks can express as:

$$\rho_D = \frac{U(\tau, W)}{Z_U}, \tag{6}$$

where $Z_U = Tr(U(\tau, W))$ is the trace of the statistical propagation operator. It is straightforward to demonstrate that ρ_D is a positive semi-definite matrix with a trace equal to 1 [36]. Therefore, the von Neumann entropy of the directed network is defined as:

$$S_D^\tau = -Tr(\rho_D log_2\rho_D). \tag{7}$$

As illustrated in the Fig. 1(B), we define the entanglement of node v_i at time τ in the directed network as:

$$DNE(\tau, v_i) = S_D^\tau(G') + S_D^\tau(G_{v_i}) - S_D^\tau(G), \tag{8}$$

where G' denotes the network after removing node v_i and its associated edges, and G_{v_i} represents the subnetwork consisting of node v_i and its connected edges. The parameter τ allows us to study *DNE* across different time scales.

2.3. Dataset description

To assess the effectiveness of the proposed method, our experiments consider six directed real-world networks from various domains, including biological network (Bn-fly_1 [37] and Bio-CE-LC [37]), citation networks (SciM [38] and SmaG [38]), hyperlink networks (BG [39]), and financial networks (Econ-Beaflw [37]). All networks are obtained from publicly available databases—SNAP (http://snap.stanford.edu/data/) and the Network Repository (https://networkrepository.com/)—ensuring the reproducibility of our experiments. Basic statistics of these real-world networks are presented in Table 1.

2.4. Experimental design

We conduct targeted attack experiments on the aforementioned directed networks. Specifically, we compare the performance of *DNE* with other centrality measures, including Out degree [40], Betweenness [41], Closeness [42], Eigenvector [43], BII [44], and Random removal [45], in dismantling both network information flow across various temporal scales ($\tau = 0.1s, 3s, 30s$) and network connectivity. For targeted attack experiments, we apply *DNE* at a small temporal scale ($\tau = 0.001s$).

To evaluate the effectiveness of various dismantling algorithms in disrupting information flow in directed networks, we quantify the dismantling rate of information flow, *FR*, by the area under the curve of *NRI* as a function of node removal, mathematically expressed as:

$$FR = \frac{1}{N}\sum_{i=1}^{N} NRI(q) \quad (q = i/N), \tag{9}$$

where q represents the fraction of nodes removed. It is important to note that after each node removal, the corresponding rows and columns of the network's adjacency matrix W are deleted, leading to changes in the network's propagation operator $G(\tau, W)$. These adjustments ensure that the metric reflects the dynamic impact of node removal on the network's information propagation capacity.

For dismantling network connectivity, similar to undirected networks [46], we use the largest weakly connected component, $S(q)$, to measure the connectivity of directed networks. The dismantling rate of connectivity, denoted as Schneider R [47], is quantified by the area under the curve of the relative size of the largest weakly connected component, defined as $s(q) = S(q)/N$, as a function of node removal. Mathematically, it is expressed as:

$$R = \frac{1}{N}\sum_{i=1}^{N} s(q) \quad (q = i/N), \tag{10}$$

To highlight the superior effectiveness of our method, we define the promotion ratios φ, which quantify the relative improvement of our approach over established benchmarks:

$$\varphi^{FR} = \frac{\left(FR^{best}{}_{benchmarks} - FR^{best}{}_{our\ methods}\right)}{FR^{best}{}_{benchmarks}} \times 100\%. \tag{11}$$

Table 1
Basic statistics of real-world networks.

Networks	N	M	$\langle k\rangle$	$\langle c\rangle$	$\langle D\rangle$
Econ-Beaflw	502	52999	211.1514	0.5114	0.2107
Bn-fly _1	1781	9630	10.8145	0.1450	0.0030
SciM	2729	10412	7.6306	0.0855	0.0014
BG	1224	19022	31.0817	0.2184	0.0127
Bio-CE-LC	1387	1648	2.3764	0.0379	0.0009
SmaG	1024	4918	9.6055	0.1540	0.0047

Note: N-network size, M-number of edges, $\langle k\rangle$- average degree, $\langle c\rangle$-clustering coefficient, $\langle D\rangle$-network density.

$$\varphi^{R} = \frac{\left(R^{best}{}_{benchmarks} - R^{best}{}_{our\ methods}\right)}{R^{best}{}_{benchmarks}} \times 100\%. \tag{12}$$

3. Results

3.1. The effect of temporal scale τ

As the temporal scale τ increases, the range of information flow within the network expands, eventually allowing information to propagate almost all nodes. Consequently, the propagation operator $G(\tau, W)$ tends to reach a steady-state distribution, and *DNE* is significantly impacted. In this section, we primarily investigate how τ affects the ability of *DNE* to dismantle the network information flow and network connectivity in directed networks.

3.1.1. The effect of temporal scale τ on DNE

We first investigate the effect of the temporal scale τ on the variation of *DNE*, using the SmaG network as a case study. In this experiment, we control τ from 0 to 50 s, with an interval of 0.1 s, and compute *DNE* for all nodes in the network across different τ.

As shown in Fig. 2(A), *DNE* gradually increase as the temporal scale τ increases, eventually reaching a steady state. At smaller temporal scales, *DNE* fluctuate significantly, indicating a limited range of information flow and strong locality in node interactions. As τ increases, the influence of information flow gradually spreads across more nodes in the network, leading to the stabilization of *DNE*. Specifically, once τ surpasses a certain threshold, the pattern of information flow tends to equilibrate, and *DNE* of most nodes no longer fluctuate significantly, indicating that the network's information flow has reached equilibrium at larger temporal scales. Furthermore, different nodes exhibit varying *DNE* trends as τ increases. Most nodes with high Out degrees display a marked increase in their *DNE* values with increasing τ, ultimately reaching relatively high steady-state values. In contrast, nodes with low Out degrees tend to exhibit only gradual changes in *DNE* over time, resulting in comparatively lower steady-state values.

3.1.2. The effect of temporal scale τ on network dismantling

In this section, we investigate the effect of *DNE* at different temporal scales on dismantling both the information flow and connectivity of directed networks, using the SmaG network as an example. Our results indicate that *DNE* at a small temporal scale is more effective in dismantling both network information flow and connectivity.

Firstly, we assess the performance of *DNE* at small, medium, and large temporal scales ($\tau = 0.1s, 3s, 30s$) in dismantling network information flow. As shown in Fig. 2(B, a–c), *DNE* at small temporal scales effectively identifies critical nodes for information flow across all temporal scales. Consequently, when these nodes are removed, the network's *NRI* decreases more rapidly, reflecting a significant disruption in network information interchange. Additionally, we investigated the impact of *DNE* on network connectivity at different temporal scales. As shown in Fig. 2(B, d), *DNE* at smaller temporal scales lead to a more rapid decline in $s(q)$. When the top 30 % of nodes, as identified by *DNE* at different temporal scales, are removed, the smallest $s(q)$ is achieved under the smaller temporal scale condition. This demonstrates that *DNE* evaluated at shorter temporal scales is particularly effective in fragmenting network connectivity.

3.2. Approximate calculation of DNE at small temporal scale

Considering the high time complexity of *DNE*, we approximate S_D at a small temporal scale using mean-field theory [48] in this section. Given that the density matrix can be diagonalized as $\rho_D = Q(\Lambda/Z)Q^{\dagger}$. Thus, we can express S_D as:

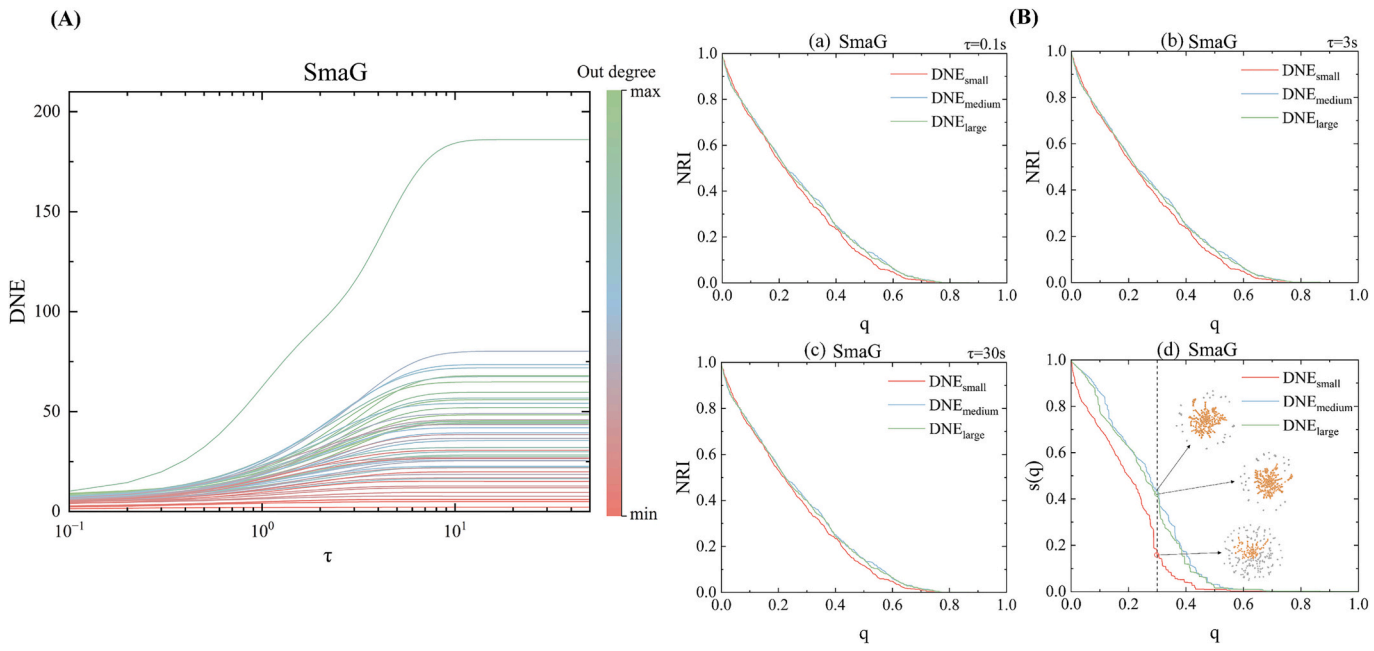

Fig. 2. The effect of temporal scale τ on the SmaG network. (A) Influence of τ on *DNE* values. (B, a–c) Impact of *DNE* at different temporal scales on dismantling information flow. (B, d) Impact of *DNE* at different temporal scales on dismantling connectivity.

$$\begin{aligned} S_D &= -Tr(\rho_D log_2 \rho_D) \\ &= -Tr((\Lambda/Z) log_2(\Lambda/Z)) \\ &= -\sum_{i=1}^{N} \frac{\lambda_i}{Z} log_2\left(\frac{\lambda_i}{Z}\right), \end{aligned} \tag{13}$$

where λ_i is the eigenvalue of $U(\tau, W)$. Switching to natural logarithms and converting the base, we have:

$$\begin{aligned} S_D &= -\sum_{i=1}^{N} \frac{\lambda_i}{Z} \frac{ln(\lambda_i/Z)}{ln2} \\ &= -\frac{1}{ln2} \sum_{i=1}^{N} \frac{\lambda_i}{Z} ln\left(\frac{\lambda_i}{Z}\right) \\ &= \frac{1}{ln2}\left(-\sum_{i=1}^{N} \frac{\lambda_i}{Z} ln(\lambda_i) + lnZ \right). \end{aligned} \tag{14}$$

Using the mathematical properties of ρ_D, we establish the relationship:

$$\sum_{i=1}^{N} \frac{\lambda_i}{Z} ln(\lambda_i) = Tr(\rho_D ln(U(\tau, W))). \tag{15}$$

When τ is very small, ignoring higher-order noncommutative terms, we approximate $U(\tau, W) = e^{-\tau L_s}/N$, where $L_s = H + H^{\dagger} = 2I - P - P^{\dagger}$ is a real symmetric matrix. Expanding $ln(U(\tau, W))$, we find it equals $-\tau L_s - lnN$. Thus, we have: $\sum_{i=1}^{N} \frac{\lambda_i}{Z} ln(\lambda_i) = Tr(\rho_D(-\tau L_s - lnN)) = -\tau Tr(L_s \rho_D) - lnN$, since $Tr(\rho_D) = 1$. So, we obtain:

$$S_D = \frac{1}{ln2}(\tau Tr(L_s \rho) + lnN + lnZ). \tag{16}$$

Using the eigenvalue decomposition of ρ_D, we express:$Tr(L_s \rho_D) = \sum_{i=1}^{N} \nu_i(\tau) \langle u_i | L_s | u_i \rangle$, where $\langle u_i | L_s | u_i \rangle = u_i^{\dagger} L_s u_i = \lambda_s^i$ and $\nu_i(\tau) = \lambda_i/Z$, with λ_s^i being the eigenvalues of L_s. Thus $Tr(L_s \rho_D) = \sum_{i=1}^{N} \lambda_s^i \nu_i(\tau)$. Through mean field theory, we have:

$$\begin{aligned} \langle \lambda_s \nu(\tau) \rangle &= \langle \lambda_s - \bar{\lambda}_s + \bar{\lambda}_s \rangle \langle \nu(\tau) - \bar{\nu}(\tau) + \bar{\nu}(\tau) \rangle \\ &= \bar{\lambda}_s \bar{\nu}(\tau) + \langle (\lambda_s - \bar{\lambda}_s)(\nu(\tau) - \bar{\nu}(\tau)) \rangle \\ &\approx \bar{\lambda}_s \bar{\nu}(\tau). \end{aligned} \tag{17}$$

Regarding $\bar{\lambda}_s$, we first compute the trace of L_s: $Tr(L_s) = Tr(2I - P - P^{\dagger}) = 2N - Tr(P) - Tr(P^{\dagger})$. Since $P^{\dagger}$ is the conjugate transpose of P, and $Tr(P) = Tr(P^{\dagger})$. Because the network has no self-loops, $Tr(P) = \sum_{i=1}^{N} P_{ii} = 0$. Therefore, $Tr(L_s) = 2N$, which means $\sum_{i=1}^{N} \lambda_s^i = 2N$. Thus, we can express:

$$\bar{\lambda}_s = \frac{1}{N - C} \sum_{i=C+1}^{N} \lambda_s^i = \frac{2N}{N - C}, \tag{18}$$

where C is the number of strong connected components.

Regarding $\bar{\nu}(\tau)$, the eigenvalues of the density matrix ρ_D are $\nu_i(\tau) = \lambda_i/Z$. The eigenvalues of $U(\tau, W)$ are approximately as $\lambda_i = e^{-\tau \lambda_s^i}/N$. And the partition function $Z = Tr(U(\tau, W)) = \sum_{i=1}^{N} e^{-\tau \lambda_s^i}/N$. Therefore, we get:

$$\begin{aligned} \bar{\nu}(\tau) &= \frac{1}{N - C} \sum_{C+1}^{N} \nu_i(\tau) \\ &= \frac{1}{N - C} \frac{S}{C + S}, \end{aligned} \tag{19}$$

where $S = \sum_{i=C+1}^{N} e^{-\tau \lambda_s^i}$. Consider of $C \ll N$, $\bar{\lambda}_s \approx 2$, we get:

$$Tr(L_s \rho) \approx \frac{2S}{C + S}. \tag{20}$$

Finally, substituting back into Eq. (16):

$$S_D^{MF} \approx \frac{2\tau S}{ln2(C + S)} + log_2(ZN). \tag{21}$$

Compared to the exact calculation, the approximation calculation reduces two additional matrix exponential operations (to compute the propagator $G(\tau, W)$ and its conjugate matrix $G(\tau, W)^{\dagger}$) and one matrix multiplication (multiplying $G(\tau, W)$ and $G(\tau, W)^{\dagger}$), both of which have a temporal complexity of $O(N^3)$.

We approximate S_D^{MF} at $\tau = 0.001s$ and use this approximation to calculate the *DNE* value. For each network, we calculate both the exact and approximated *DNE* values for all nodes and perform Pearson correlation analysis. The results, as shown in Fig. 3, reveal a strong correlation between the approximated and exact *DNE* values, with Pearson

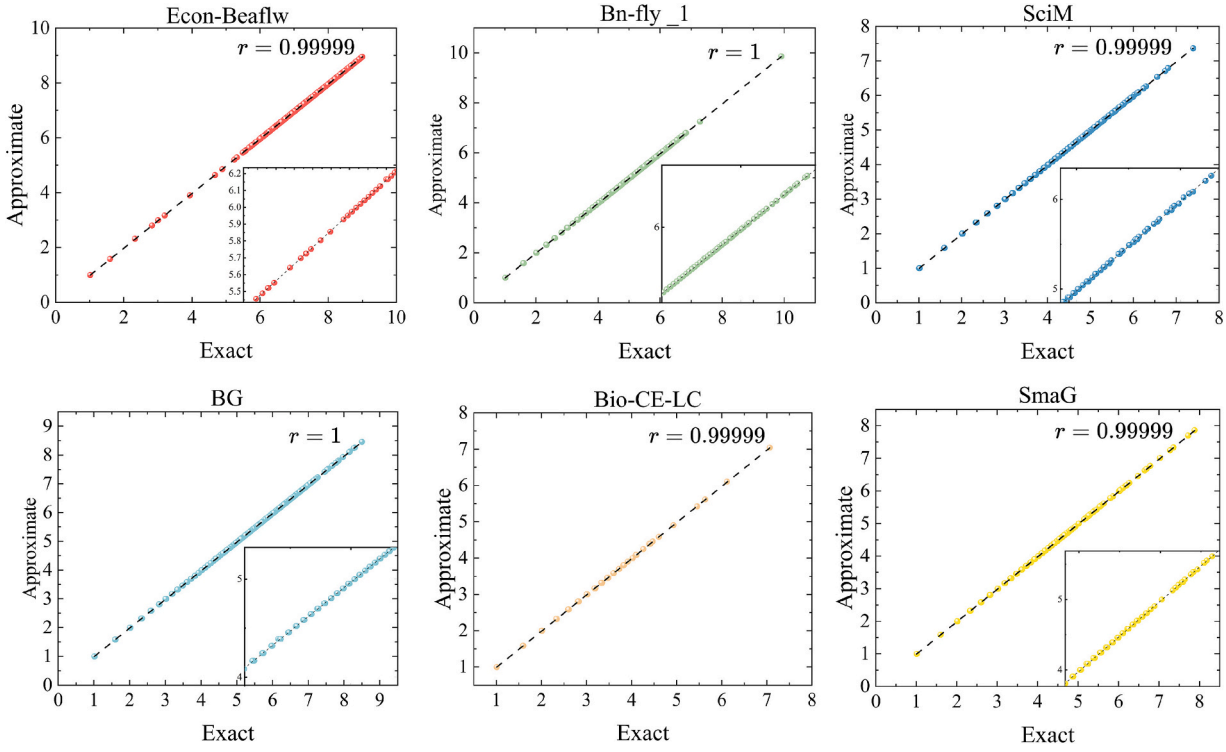

Fig. 3. Analysis of the approximated *DNE*.

correlation coefficients consistently close to 1. This demonstrates that the approximation approach is reliable and preserves the accuracy of *DNE* calculations with very small temporal scale. Moreover, we use the approximate values of *DNE* in the network dismantling experiments conducted in our study.

3.3. The performance of DNE in dismantling information flow

As summarized in Table 2, *DNE* consistently outperforms all benchmarks, demonstrating its superior effectiveness in dismantling information flow in directed networks. Notably, *DNE* performs best in biological networks, achieving substantial improvement rates in comparison to other centrality measures. For example, in the Bio-CE-LC and Bn-fly_1 networks, *DNE* achieves improvement rates of 17.35 % and 21.23 % at small temporal scales, 17.35 % and 21.21 % at medium temporal scales, and 17.35 % and 21.34 % at large temporal scales, respectively. Moreover, the performance of *DNE* in citation networks (SciM and SmaG) is relatively modest, with improvement rates hovering around 5 % across all temporal scales. Moreover, in the financial network (Econ-Beaflw), *DNE*'s performance is less pronounced, with improvement rates below 4 % at all temporal scales.

As shown in Figs. 4–6, we illustrate the evolution of $S(q)$ as nodes are removed under different algorithms in networks at small temporal scales. From the results, it is clear that *DNE* consistently outperforms all other centrality measures across all tested networks. This superiority is particularly evident in biological networks such as Bn-fly_1 and Bio-CE-LC, where *DNE* exhibits a significantly steeper decline in *NRI* compared to benchmarks, reflecting its strong ability to dismantle network

Table 2
Comparison of dismantling algorithms of *FR* at different temporal scale.

Network	τ(s)	Out degree	Closeness	Eigen vector	Betweenness	BII	Random	*DNE*	φ_{FR}
Econ-Beaflw	0.1	0.460	0.435	0.437	0.463	0.442	0.474	**0.418**	**3.91 %**
	3	0.460	0.433	0.435	0.463	0.440	0.474	**0.417**	**3.85 %**
	30	0.461	0.435	0.437	0.463	0.441	0.474	**0.418**	**3.92 %**
Bn-fly _1	0.1	0.263	0.228	0.232	0.249	0.230	0.420	**0.180**	**21.23 %**
	3	0.263	0.227	0.231	0.250	0.229	0.419	**0.179**	**21.21 %**
	30	0.263	0.228	0.232	0.249	0.230	0.420	**0.180**	**21.34 %**
SciM	0.1	0.271	0.327	0.341	0.275	0.408	0.380	**0.256**	**5.49 %**
	3	0.271	0.327	0.342	0.275	0.408	0.380	**0.256**	**5.57 %**
	30	0.271	0.327	0.342	0.275	0.408	0.380	**0.256**	**5.57 %**
BG	0.1	0.359	0.270	0.272	0.302	0.261	0.472	**0.249**	**4.87 %**
	3	0.357	0.262	0.264	0.301	0.254	0.471	**0.244**	**3.97 %**
	30	0.358	0.265	0.267	0.302	0.256	0.472	**0.246**	**4.02 %**
Bio-CE-LC	0.1	0.149	0.222	0.272	0.166	0.348	0.349	**0.123**	**17.35 %**
	3	0.149	0.222	0.272	0.166	0.348	0.349	**0.123**	**17.35 %**
	30	0.149	0.222	0.272	0.166	0.348	0.349	**0.123**	**17.35 %**
SmaG	0.1	0.261	0.346	0.368	0.259	0.345	0.440	**0.244**	**5.49 %**
	3	0.261	0.346	0.368	0.259	0.345	0.440	**0.244**	**5.49 %**
	30	0.261	0.346	0.368	0.259	0.345	0.440	**0.244**	**5.49 %**

Bold values indicate the best performance achieved among all compared methods, as well as the corresponding percentage improvement brought by the best-performing algorithm.

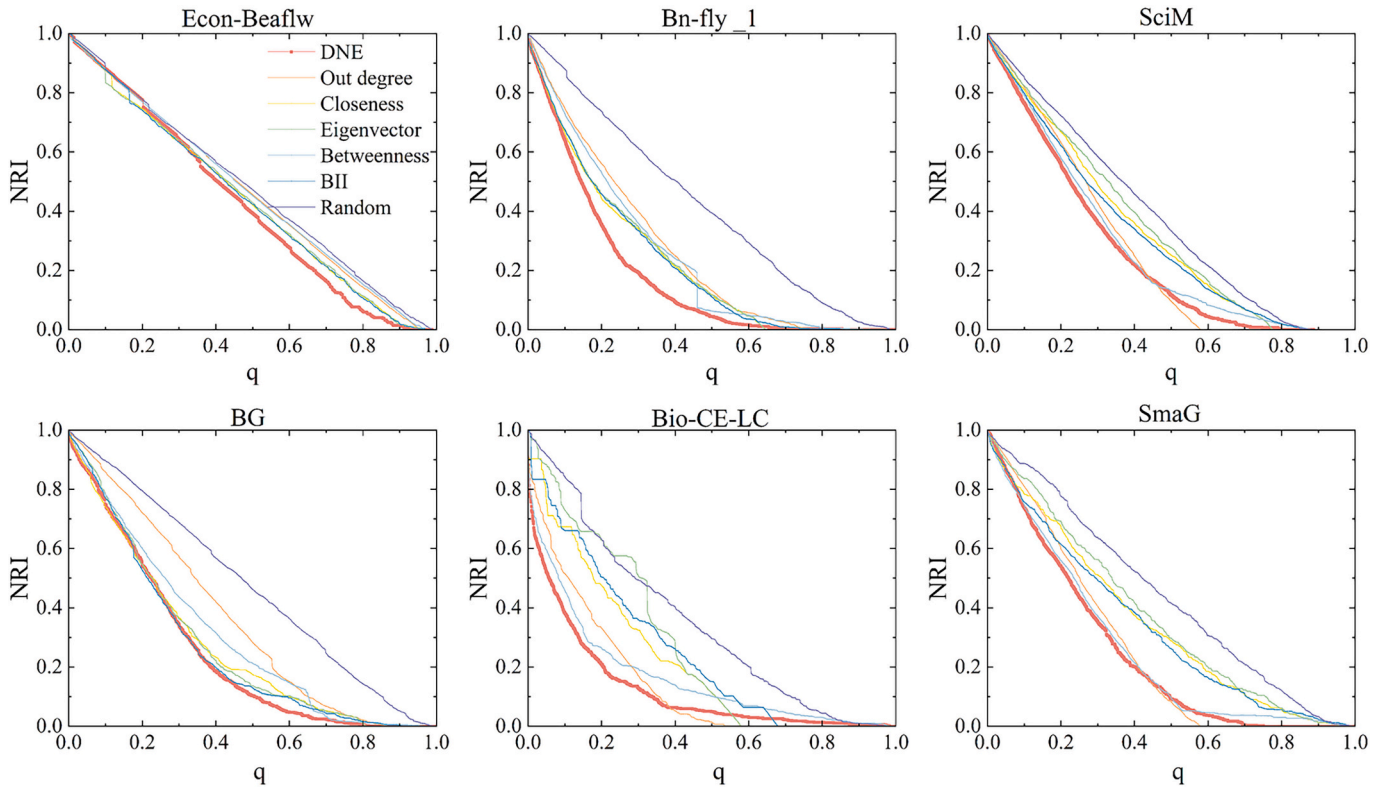

Fig. 4. Comparison the *NRI* of different dismantling algorithms on small temporal scale.

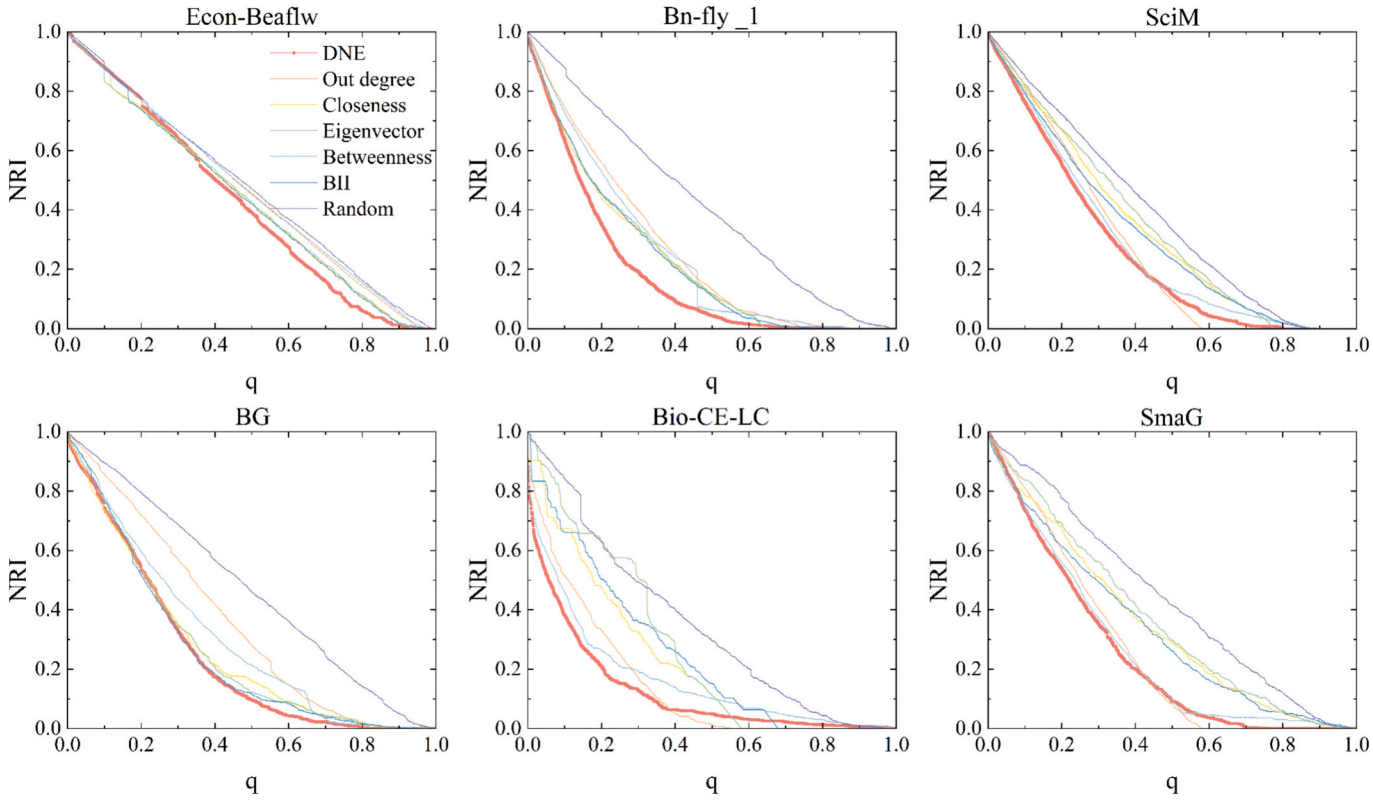

Fig. 5. Comparison the *NRI* of different dismantling algorithms on medium temporal scale.

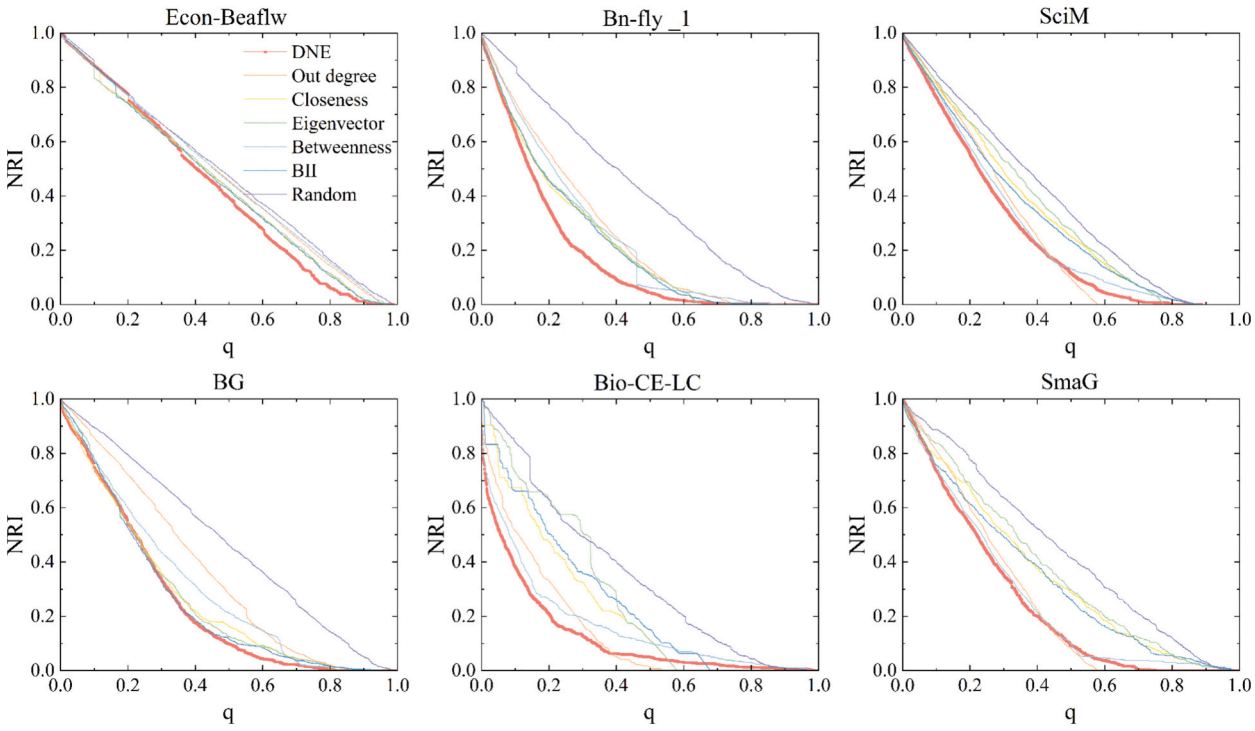

Fig. 6. Comparison the *NRI* of different dismantling algorithms on large temporal scale.

functionality. In contrast, for networks like Econ-Beaflw and BG, while *DNE* still performs better, the difference between *DNE* and benchmarks is less pronounced, suggesting that the relative improvement of *DNE* may depend on the structural properties of the network. These results highlight the robustness and adaptability of *DNE*, showing its ability to effectively target key nodes to dismantle the functionality of various types of networks.

3.4. The performance of DNE in dismantling connectivity

In this section, we evaluate the performance of *DNE* in dismantling network connectivity. As shown in Table 3, the experimental results indicate that *DNE* outperforms benchmarks across various real-world networks. Overall, *DNE* consistently produces smaller remaining network sizes, demonstrating a more efficient disruption of network connectivity. For instance, while the Econ-Beaflw and SmaG networks show marginal improvements of 2.93 % and 3.04 %, respectively, the Bn-fly_1 and Bio-CE-LC networks exhibit dramatic improvements of 36.00 % and 40.39 %. In the SciM and BG networks, *DNE* achieves notable improvements of 8.87 % and 10.38 % over benchmarks.

Additionally, we analyze the evolution of the $s(q)$ throughout the dismantling process. As shown in Fig. 7, *DNE* consistently produces a steeper decline in $s(q)$ compared to other strategies, indicating its superior ability to disrupt connectivity. For example, in the Bn-fly_1 and Bio-CE-LC networks, the $s(q)$ curve under *DNE* drops sharply, reflecting its effectiveness in networks with structurally critical nodes. In contrast, random removal shows the slowest decline, underscoring the advantage of targeted node removal.

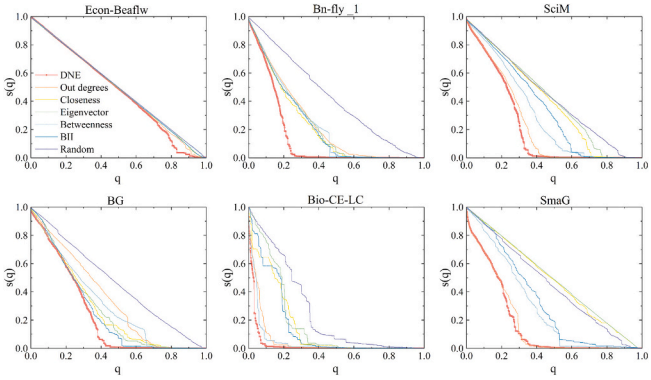

Fig. 7. Comparison the $s(q)$ of different algorithms on real-world networks.

Furthermore, using SmaG as an example, we compare the performance of *DNE* with other node centrality metrics at a specific stage of network dismantling. Specifically, we removed the top 25 % of nodes deemed most critical by each algorithm and measured $s(q)$ in the resulting network. As shown in Fig. 8, under *DNE*, $s(q)$ drops to 236,

Table 3
Comparison of dismantling algorithms of Schneider *R*.

Network	Out degree	Closeness	Eigenvector	Betweenness	BII	Random	*DNE*	φ_R
Econ-Beaflw	0.486	0.487	0.488	0.495	0.487	0.496	**0.472**	**2.93 %**
Bn-fly _1	0.238	0.215	0.226	0.229	0.219	0.426	**0.137**	**36.00 %**
SciM	0.227	0.391	0.410	0.296	0.344	0.428	**0.207**	**8.87 %**
BG	0.343	0.274	0.275	0.308	0.255	0.462	**0.228**	**10.38 %**
Bio-CE-LC	0.054	0.149	0.175	0.049	0.145	0.259	**0.029**	**40.39 %**
SmaG	0.174	0.479	0.487	0.288	0.327	0.448	**0.168**	**3.04 %**

Bold values indicate the best performance achieved among all compared methods, as well as the corresponding percentage improvement brought by the best-performing algorithm.

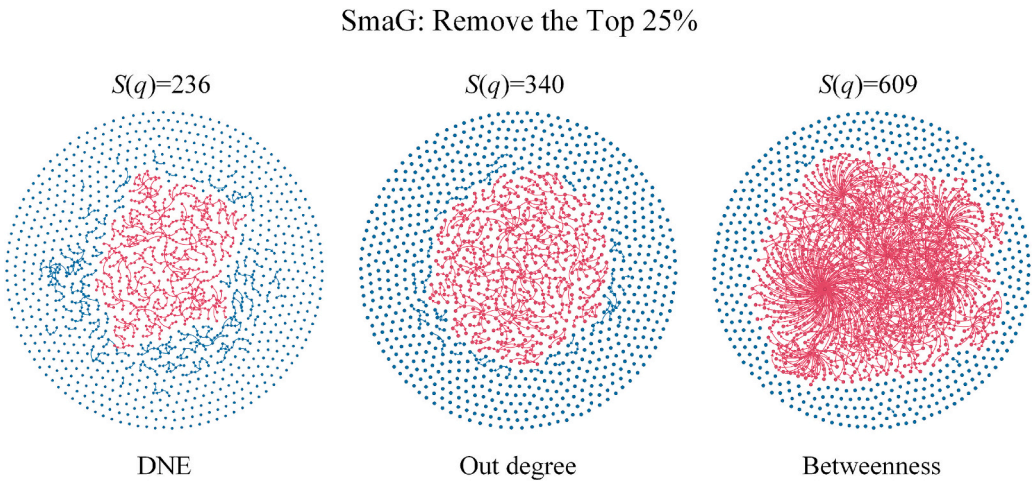

Fig. 8. Network dismantling performance using various algorithms by removing the top 25 % of nodes, where the red component represents the largest connected component in the current network. (For interpretation of the references to color in this figure legend, the reader is referred to the web version of this article.)

whereas the Out degree and Betweenness strategies yield $s(q)$ of 340 and 609, respectively. In other words, *DNE* reduces $s(q)$ by 104 nodes more than Out degree and by 373 nodes more than Betweenness, corresponding to improvements of 31.18 % and 61.25 %, respectively. These findings suggest that *DNE* provides a robust approach for identifying and removing key nodes to effectively fragment networks.

3.5. Correlation analysis

To investigate the correlation between different node centrality metrics, we employed Kendall's Tau coefficient [49] to compare *DNE* with several typically used centrality measures. As a rank-based correlation measure, Kendall's Tau quantifies the degree of consistency in the relative ordering of nodes across different centrality metrics. Specifically, we compute the values of all centrality metrics for each node in the SmaG network and then calculate the Kendall's Tau coefficients based on the rank order of these metrics. As shown in Fig. 9(A), *DNE* exhibits the strongest relationships with Out degree ($K = 0.606$) and Betweenness ($K = 0.571$), indicating that it emphasizes both the number of outgoing connections from a node and its bridging or mediating role within the network. By contrast, *DNE* shows moderate or lower correlations with Closeness ($K = 0.304$), Eigenvector ($K = 0.243$), and BII ($K = 0.483$). This pattern suggests that *DNE* is relatively distinct from measures focusing on global proximity (Closeness) or connectivity to influential nodes (Eigenvector). In other words, while *DNE* captures certain aspects of node influence, it does not heavily depend on a node's shortest-path distances or its links to highly ranked neighbors. Conceptually, nodes with high *DNE* values tend to exhibit significant outward reach (high Out degree) and occupy crucial intermediary positions (high Betweenness). Consequently, *DNE* can highlight nodes that actively shape information or resource flow by serving as both a conduit and a source. Its moderate correlations with other centralities imply that *DNE* can complement these measures by providing an alternative view of network influence.

As shown in Fig. 9(B), we conducted a visual analysis of *DNE* alongside other centrality measures by arranging node positions based on Out degree values—a layout that remains consistent across all figures—while adjusting node color and size according to each respective centrality measure. In the Out degree, nodes with higher Out degree generally occupy more prominent central positions. In Betweenness, some nodes at similar positions also stand out, indicating intermediary or bridging roles in information flow. The Closeness reveals relatively clustered red nodes, suggesting shorter paths to other nodes. Although the Eigenvector distribution is similar to that of Closeness, the wider

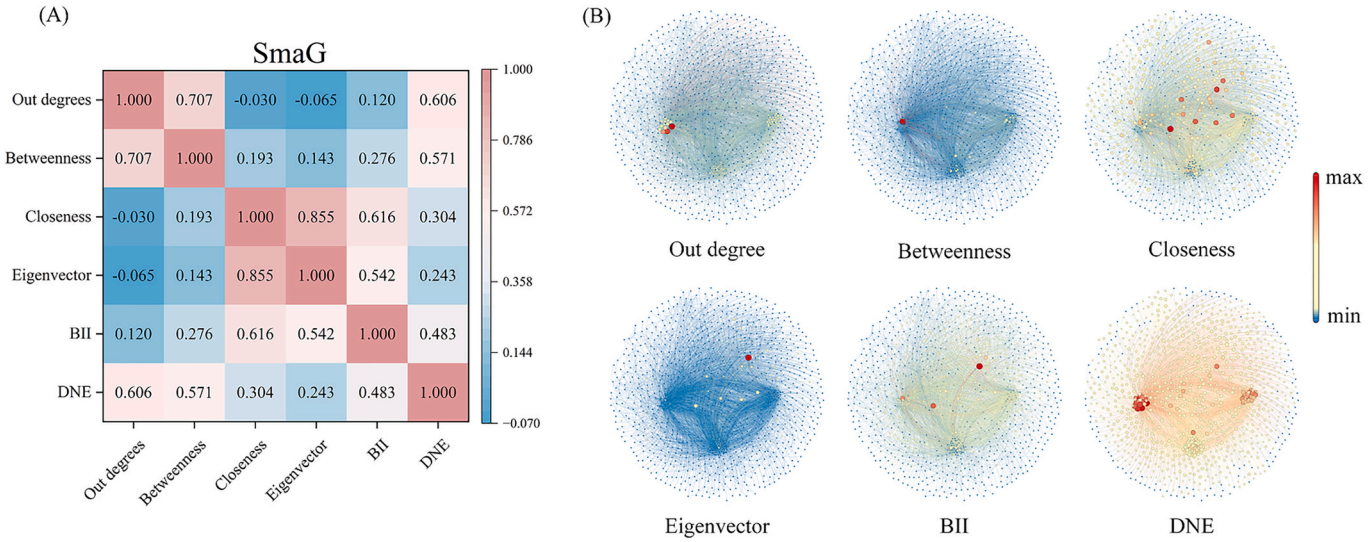

Fig. 9. Correlation analysis.

range of centrality values results in some nodes appearing blue rather than red. The BII measure partially overlaps with Eigenvector but exhibits its own unique high-centrality pattern. Finally, *DNE* combines outward connectivity and bridging status, aligning high-value nodes with those in Out degree and Betweenness. Moreover, differences in *DNE* values are less pronounced, resulting in a noticeably larger proportion of red and yellow nodes. Overall, *DNE* simultaneously accounts for both high outward connectivity and bridging potential, thereby offering a distinct perspective on node importance within directed networks.

4. Conclusion and discussion

In this study, we address the directionality of information flow by employing random walks to model the dynamic interactions among nodes, thereby constructing an information field model for directed networks. Additionally, we introduce the *NRI* to evaluate a network's information flow capacity. Leveraging the generalized network density matrix for directed networks, we derive the *DNE* centrality metric. We further examine how varying temporal scales influence *DNE* performance and observe that its effectiveness is enhanced at smaller temporal scales. To reduce the computational complexity of *DNE*, we build on this insight and employ mean-field theory to approximate *DNE* under small temporal scales. Extensive experiments show that *DNE*, evaluated at a small temporal scale, efficiently dismantles both information flow and connectivity in directed networks. Finally, correlation analyses between *DNE* at a small temporal scale and other node centrality metrics provide deeper insights into its behavior and interrelationships.

Our main contribution lies in extending the task of dismantling information flow to directed networks while addressing several key challenges. For instance, we construct a generalized network density matrix to handle cases where the control operator is non-Hermitian. We also redefine how the capacity of information flow is quantified to ensure a monotonically decreasing metric (*NRI*) as nodes are removed. Moreover, using mean-field theory, we approximate *DNE* at small temporal scales and demonstrate strong consistency with exact values.

Nevertheless, while the random walk approach effectively captures directional interactions, it remains a relatively generic model. In various systems—such as neural networks, epidemic processes, or birth-death processes—more specialized dynamic models may better capture the nuances of information flow. Furthermore, although the *DNE* approximation method significantly reduces computation time, its overall time complexity remains high. An important direction for future research is to develop new algorithms that can efficiently and effectively dismantle information flow in multilayer networks, higher-order networks, and other complex network structures.

CRediT authorship contribution statement

Min Wu: Conceptualization, Methodology, Software, Visualization, Writing – original draft. **Jianhong Mou:** Writing – review & editing. **Bitao Dai:** Visualization. **Suoyi Tan:** Writing – review & editing. **Xin Lu:** Conceptualization, Funding acquisition, Supervision, Writing – review & editing.

Declaration of competing interest

The authors declare that they have no known competing financial interests or personal relationships that could have appeared to influence the work reported in this paper.

Acknowledgements

This work is supported by the National Natural Science Foundation of China (72025405, 72474223, 72421002), the Science and Technology Innovation Program of Hunan Province (2023JJ40685, 2024JJ6069, 2024RC3133), and the Humanities and Social Sciences Research project of Ministry of Education of China (24YJC630128).

Data availability

Data will be made available on request.

References

[1] Tu Y. How robust is the Internet? Nature 2000;406:353–4.
[2] Lin J, Ban Y. Complex network topology of transportation systems. Transp Rev 2013;33:658–85.
[3] Milanović JV, Zhu W. Modeling of interconnected critical infrastructure systems using complex network theory. IEEE Trans Smart Grid 2017;9:4637–48.
[4] Battiston S, Caldarelli G, May RM, Roukny T, Stiglitz JE. The price of complexity in financial networks. Proc Natl Acad Sci 2016;113:10031–6.
[5] Gosak M, Markovič R, Dolenšek J, Rupnik MS, Marhl M, Stožer A, et al. Network science of biological systems at different scales: a review. Phys Life Rev 2018;24:118–35.
[6] Liu Y-Y, Barabási A-L. Control principles of complex systems. Rev Mod Phys 2016;88:035006.
[7] Braunstein A, Dall'Asta L, Semerjian G, Zdeborová L. Network dismantling. Proc Natl Acad Sci 2016;113:12368–73.
[8] Clusella P, Grassberger P, Pérez-Reche FJ, Politi A. Immunization and targeted destruction of networks using explosive percolation. Phys Rev Lett 2016;117:208301.
[9] Arulselvan A, Commander CW, Elefteriadou L, Pardalos PM. Detecting critical nodes in sparse graphs. Comput Oper Res 2009;36:2193–200.
[10] Morone F, Makse HA. Influence maximization in complex networks through optimal percolation. Nature 2015;524:65–8.
[11] Mugisha S, Zhou H-J. Identifying optimal targets of network attack by belief propagation. Phys Rev E 2016;94:012305.
[12] Zdeborová L, Zhang P, Zhou H-J. Fast and simple decycling and dismantling of networks. Sci Rep 2016;6:37954.
[13] Ren X-L, Gleinig N, Helbing D, Antulov-Fantulin N. Generalized network dismantling. Proc Natl Acad Sci 2019;116:6554–9.
[14] Engsig M, Tejedor A, Moreno Y, Foufoula-Georgiou E, Kasmi C. DomiRank Centrality reveals structural fragility of complex networks via node dominance. Nat Commun 2024;15:56.
[15] Dai B, Mou J, Tan S, Cai M, Liljeros F, Lu X. The role of link redundancy and structural heterogeneity in network disintegration. Expert Syst Appl 2024;255:124590.
[16] Fan C, Zeng L, Sun Y, Liu Y-Y. Finding key players in complex networks through deep reinforcement learning. Nat Mach Intell 2020;2:317–24.
[17] Grassia M, De Domenico M, Mangioni G. Machine learning dismantling and early-warning signals of disintegration in complex systems. Nat Commun 2021;12:5190.
[18] Manke T, Demetrius L, Vingron M. An entropic characterization of protein interaction networks and cellular robustness. J R Soc Interface 2006;3:843–50.
[19] Dunne JA, Williams RJ, Martinez ND. Network structure and biodiversity loss in food webs: robustness increases with connectance. Ecol Lett 2002;5:558–67.
[20] Doyle JC, Alderson DL, Li L, Low S, Roughan M, Shalunov S, et al. The "robust yet fragile" nature of the Internet. Proc Natl Acad Sci 2005;102:14497–502.
[21] Kim J, Ladosz P, Oh H. Optimal communication relay positioning in mobile multi-node networks. Robot Auton Syst 2020;129:103517.
[22] Ghavasieh A, Nicolini C, De Domenico M. Statistical physics of complex information dynamics. Phys Rev E 2020;102:052304.
[23] Gao J, Barzel B, Barabási A-L. Universal resilience patterns in complex networks. Nature 2016;530:307–12.
[24] Barzel B, Barabási A-L. Universality in network dynamics. Nat Phys 2013;9:673–81.
[25] Harush U, Barzel B. Dynamic patterns of information flow in complex networks. Nat Commun 2017;8:2181.
[26] Ghavasieh A, De Domenico M. Diversity of information pathways drives sparsity in real-world networks. Nat Phys 2024;20:512–9.
[27] Boccaletti S, Latora V, Moreno Y, Chavez M, Hwang D-U. Complex networks: structure and dynamics. Phys Rep 2006;424:175–308.
[28] Masuda N, Klemm K, Eguíluz VM. Temporal networks: slowing down diffusion by long lasting interactions. Phys Rev Lett 2013;111:188701.
[29] Rosvall M, Bergstrom CT. Maps of random walks on complex networks reveal community structure. Proc Natl Acad Sci 2008;105:1118–23.
[30] Newman ME. A measure of betweenness centrality based on random walks. Social Netw 2005;27:39–54.
[31] Ghavasieh A, Stella M, Biamonte J, De Domenico M. Unraveling the effects of multiscale network entanglement on empirical systems. Commun Phys 2021;4:129.
[32] Ghavasieh A, Bertagnolli G, De Domenico M. Dismantling the information flow in complex interconnected systems. Phys Rev Res 2023;5:013084.
[33] Garlaschelli D, Loffredo MI. Patterns of link reciprocity in directed networks. Phys Rev Lett 2004;93:268701.
[34] Noh JD, Rieger H. Random walks on complex networks. Phys Rev Lett 2004;92:118701.
[35] De Domenico M, Biamonte J. Spectral entropies as information-theoretic tools for complex network comparison. Phys Rev X 2016;6:041062.

[36] Ghavasieh A, De Domenico M. Generalized network density matrices for analysis of multiscale functional diversity. Phys Rev E 2023;107:044304.
[37] Rossi R, Ahmed N. The network data repository with interactive graph analytics and visualization. In: Proceedings of the AAAI conference on artificial intelligence; 2015.
[38] Batagelj V, Pajek Mrvar A. Citeseer. 2014.
[39] Kunegis J. Konect: the koblenz network collection. In: Proceedings of the 22nd international conference on world wide web; 2013. p. 1343–50.
[40] Holme P, Kim BJ, Yoon CN, Han SK. Attack vulnerability of complex networks. Phys Rev E 2002;65:056109.
[41] Granovetter MS. The strength of weak ties. Am J Sociol 1973;78:1360–80.
[42] Freeman LC. Centrality in social networks: conceptual clarification. Social network: critical concepts in sociology1. Londres: Routledge; 2002. p. 238–63.
[43] Bonacich P. Factoring and weighting approaches to status scores and clique identification. J Math Sociol 1972;2:113–20.
[44] Lee Y-L, Wen Y-F, Xie W-B, Pan L, Du Y, Zhou T. Identifying influential nodes on directed networks. Inform Sci 2024;120945.
[45] Albert R, Jeong H, Barabási A-L. Error and attack tolerance of complex networks. Nature 2000;406:378–82.
[46] Callaway DS, Newman ME, Strogatz SH, Watts DJ. Network robustness and fragility: percolation on random graphs. Phys Rev Lett 2000;85:5468.
[47] Schneider CM, Moreira AA, Andrade Jr JS, Havlin S, Herrmann HJ. Mitigation of malicious attacks on networks. Proc Natl Acad Sci 2011;108:3838–41.
[48] Barabási A-L, Albert R, Jeong H. Mean-field theory for scale-free random networks. Phys A: Stat Mech Appl 1999;272:173–87.
[49] Kendall MG. A new measure of rank correlation. Biometrika 1938;30:81–93.